scientific reports

Check for updates

OPEN

Effect of nHA/CS/PLGA delivering adipose stem cell-derived exosomes and bone marrow stem cells on bone healing—in vitro and in vivo studies

Ting Wang[1], Shu Guo[1]✉ & Ye Zhang[2]

Adipose stem cell-derived exosomes (ADSC-EXO) have been demonstrated to promote osteogenic differentiation of bone marrow stem cells (BMSCs) and facilitate bone regeneration. The present study aims to investigate the effect of ADSC-EXO-loaded nano-hydroxyapatite/chitosan/poly-lactide-co-glycolide (nHA/CS/PLGA) scaffolds on maxillofacial bone regeneration using tissue engineering. ADSC-EXO was isolated and co-cultured with BMSCs, and the osteogenic differentiation of BMSCs was assessed through the detection of mineralized nodule formation, alkaline phosphatase (ALP) activity, and mRNA expression of COL1A1 and runt-related transcription factor 2 (RUNX2). The nHA/CS/PLGA scaffolds were fabricated and loaded with ADSC-EXO and BMSCs, and these tissue engineering complexes were applied to the maxillofacial bone defect region of rabbits to elucidate their bone regeneration effect. The osteogenic differentiation of BMSCs was markedly enhanced when they were co-cultured with ADSC-EXO. This was evidenced by an increase in the formation of mineralized nodule formation, ALP activity, and mRNA expression of COL1A1 and runt-related transcription factor 2 (RUNX2). In vivo experiments demonstrated that the application of ADSC-EXO and BMSCs loaded nHA/CS/PLGA scaffolds effectively repaired maxillofacial bone defects in rabbits. ADSC-EXO has been demonstrated to promote the osteogenic differentiation of BMSCs. The ADSC-EXO and BMSCs loaded nHA/CS/PLGA scaffolds have been shown to facilitate the regeneration of maxillofacial bone defects. This may serve as a potential therapeutic strategy for large-scale bone defects.

Keywords Adipose stem cell-derived exosomes, Bone marrow stem cells, Nanohydroxyapatite/chitosan/poly-lactic-co-glycolic acid scaffolds, Wound healing, Mandibular defect

Maxillofacial bone defects have the potential to significantly impact an individual's appearance and the functionality of the musculoskeletal system. The etiology of these defects is diverse, with periodontitis, trauma, and tumor resection representing a few of the potential causes[1]. The primary objective of maxillofacial bone defect treatment is the restoration of bone tissue. However, due to the inherent limitations in the regenerative capacity of human bone, achieving optimal outcomes presents a significant challenge[2]. The most commonly employed methodologies for the treatment of maxillofacial bone defects encompass autologous or allogeneic bone grafting, three-dimensional printing of bioscaffolds, and titanium alloy implantation[3]. While autologous bone grafting is a more efficacious method, it is not without complications. Such complications include trauma to the donor area, difficulty in survival after transplantation, and the potential for rejection reactions[4]. While three-dimensional printing technology can facilitate the creation of bespoke implants, it may present certain challenges, including intricate surgical procedures, limited biocompatibility, and the potential for additional surgical intervention[5]. In recent years, notable advancements in biomedical engineering and tissue engineering have led to substantial developments in the treatment of maxillofacial bone defects[6,7]. For example, Deng et al. discovered that hypoxic extracellular vesicles derived from mesenchymal stem cells through hypoxia treatment, in conjunction with a bioactive hydrogel, markedly enhance the formation and differentiation of

[1]Department of Plastic Surgery, The First Hospital of China Medical University, Shenyang, Liaoning 110001, PR China. [2]Department of General Surgery, The Forth Hospital of Liaoning University of Traditional Chinese Medicine, Shenyang, Liaoning 110001, PR China. ✉email: sguo@cmu.edu.cn

cranial osteoblasts, as well as local vasculogenesis and differentiation, thereby facilitating bone regeneration[8]. This finding offers novel insights and methodologies for the management of maxillofacial bone defects.

In recent years, the osteogenic differentiation potential of bone marrow mesenchymal stem cells (BMSCs) has been demonstrated to be a valuable tool in the treatment of bone defect-related diseases[9,10]. Bone tissues are dynamic, with bone formation mediated by osteoblasts and bone resorption mediated by osteoclasts, thereby maintaining a balance. Promoting osteoblast activity and reducing osteoclast activity have been evaluated as promising strategies for bone defects[11,12]. Given that BMSCs are the primary source of osteoblasts, the induction of BMSC osteogenic differentiation represents a promising approach for the repair of bone defects[13,14]. However, direct transplantation of BMSCs into maxillofacial bone defects is constrained by several factors, including phenotypic alterations of BMSCs during cell expansion, a low survival rate of transplanted cells, and a time-consuming cell culture process[15,16]. The use of tissue engineering techniques to reconstitute a physiological microenvironment for BMSCs may prove beneficial in improving outcomes.

Chitosan (CS) is an advantageous biological organic material with low immunogenicity and good biocompatibility, and has been applied in the field of tissue engineering[17]. However, its inadequate mechanical strength and accelerated degradative rate restrict its broader utilization[18,19]. Nano-hydroxyapatite (nHA) exhibits comparable crystal size, configuration and biomechanical properties to those of natural bone; however, its gradual degradation rate hinders new bone formation[20,21]. The combination of CS and nHA can compensate for the respective shortcomings of the two materials, resulting in enhanced mechanical and biological properties.

In addition to seed cells and scaffold materials, inductive factors represent a crucial element in the field of tissue engineering. Adipose tissue is currently regarded as an essential endocrine organ in the early 21st century, with documented involvement in safety, immunity, and metabolism[22]. Adipose-derived stem cells (ADSCs) are isolated from adipose tissue, which is readily accessible with minimal donor injury, and exhibit several advantageous characteristics, including high proliferative activity, non-toxicity, low immunogenicity, non-teratogenicity, and non-carcinogenicity[23]. ADSCs have been demonstrated to repair tissue defects not only through direct differentiation into target cells, but also through the secretion of paracrine agents that stimulate or induce the differentiation of neighboring immature cells[24].

Exosomes, which have a diameter of 30–150 nm, are active agents secreted by almost all cell types, including ADSCs[25]. They function as "cell-to-cell vehicles" to facilitate the transfer of active molecules, including RNAs, DNAs, and proteins, from one cell to another[26]. Recent research has confirmed that ADSC-derived exosomes (ADSC-EXO) can induce osteogenic differentiation of BMSCs and promote bone regeneration[27,28]. However, few studies have concentrated on exosomes as "inductive factors" deposited on implant surfaces. In view of these findings, our objective was to utilize ADSC-EXOs in the fabrication of tissue-engineered bones. Nevertheless, the long-term and secure delivery of ADSC-EXOs to the affected area remains a challenge. Poly-lactic-co-glycolic acid (PLGA) has a long history of use as a surgical suture material in clinical practice and has been approved by the Food and Drug Administration for human injection[29]. Furthermore, PLGA has gained prominence as a drug delivery vector in fundamental scientific research and clinical therapies due to its high drug encapsulation rate and controllable degradability[30]. The addition of PLGA represents a promising solution for the preparation of an efficacious scaffold for the delivery and release of ADSC-EXOs. Furthermore, the combination of PLGA with CS and nHA has the potential to enhance the hydrophobicity and osteogenic bioactivity of PLGA[31].

In this study, exosomes were isolated from rabbit ADSCs, immobilized into nHA/CS/PLGA scaffolds, and applied with BMSCs to maxillofacial bone defects in rabbits to investigate the therapeutic effect on bone regeneration.

Materials and methods

The protocol of methods is briefly displayed in a flowchart (Fig. 1). All the materials and instruments used in this study were listed in Table 1, as well as their suppliers.

Isolation of rabbit ADSCs and BMSCs

The 4-month-old New Zealand White rabbits (1.23 ± 1.21 kg) were purchased from Qingdao Kangda Biotechnology Co., Ltd. (Qingdao, Shandong, China). Subcutaneous adipose tissues from the groin were collected for ADSCs isolation, and bone marrow tissues from the femur and tibia were collected for BMSCs isolation. For ADSCs isolation, 150 mL lipoaspirates were washed in phosphate-buffered saline (PBS) and digested in 0.075% collagenase I (Gibco, Waltham, MA, USA) at 37 °C with constant shaking for 45 min. Dulbecco's modified Eagle's medium/F12 (DMEM) containing 10% fetal bovine serum (FBS) was then added and centrifuged at 1200 rpm for 5 min at 25 °C. After discarding the supernatant, the pellet was collected at the bottom, washed with PBS, and centrifuged twice at 1000 rpm for 5 min at 25 °C. The precipitate was then resuspended in culture media and inoculated into culture dish. To isolate BMSCs, 8 mL of a mixture of bone marrow aspirates and PBS was centrifuged at 1000 rpm for 5 min, and the supernatants were discarded. The pellets were washed with PBS and centrifuged again. The precipitate was then resuspended in culture medium and inoculated into a culture dish. Cell shape and proliferation of ADSCs and BMSCs were observed and photographed daily by inverted phase-contrast microscopy.

Identification of ADSCs and BMSCs

ADSCs (P4) were digested with 0.25% trypsin containing 0.02% EDTA after cell cultures reached 80% confluency, and then resuspended in chondrogenic medium at a density of 5×10^5 cells/ml. 0.5 ml of the cell suspension was aspirated and transferred to a 15 ml polypropylene centrifuge tube and centrifuged at 1500 rpm for 5 min. The lid of the centrifuge tube was unscrewed and cultured in an incubator (37℃, 5% CO_2) for 28 days. Then, the chondrospheres were fixed with paraformaldehyde, embedded in paraffin, sectioned and stained with Alcian blue staining solution, and then observed and photographed under a microscopy. After cell cultures reached

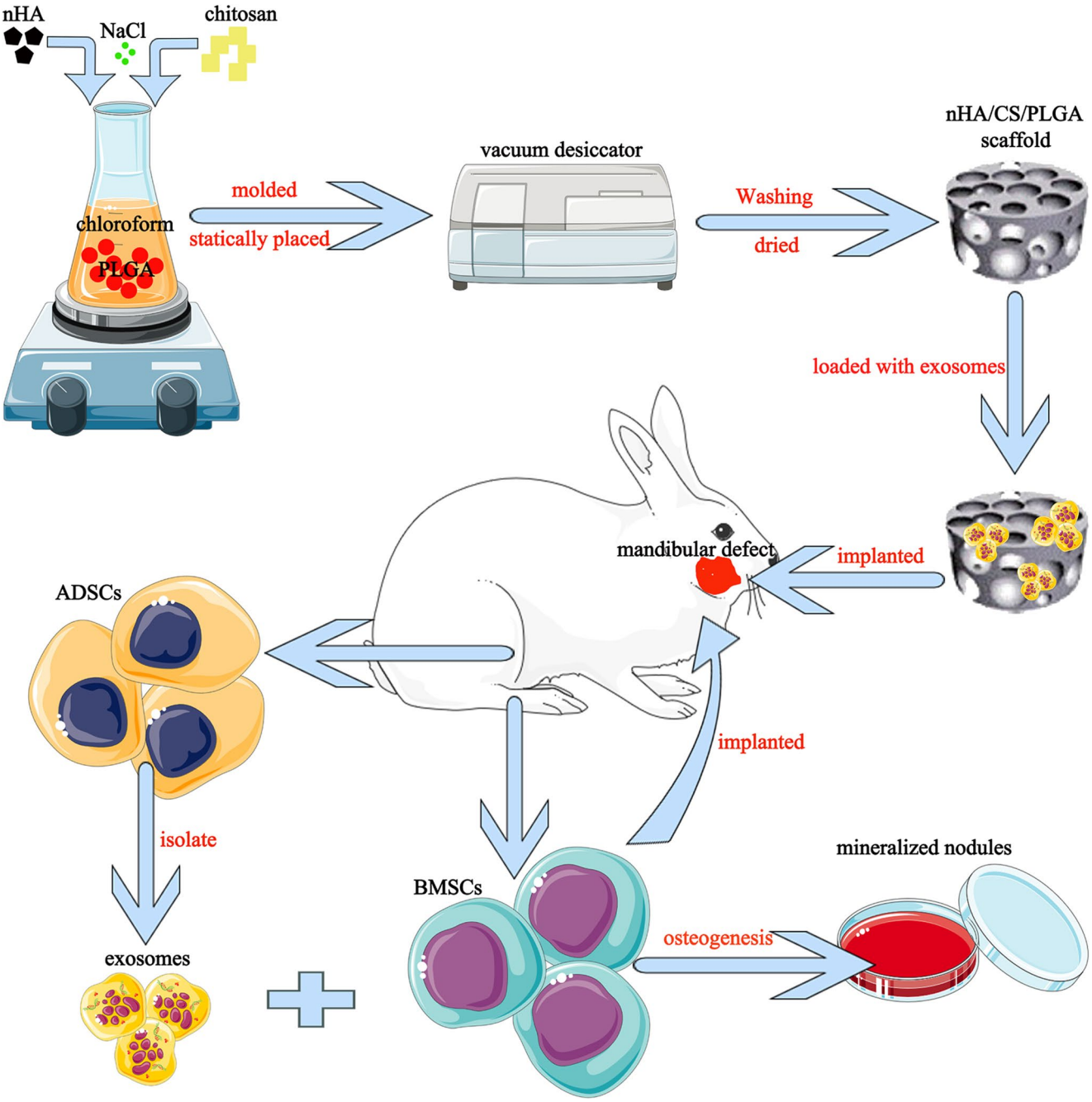

Figure 1. Flowchart of the experimental protocol.

70% confluency in 6-well plates, ADSCs (P4) were cultured in adipogenic medium for 14 days. Then cells were washed twice with PBS, fixed with paraformaldehyde for 20 min, stained with oil red O staining solution for 40 min, washed twice with isopropanol, washed with PBS, and observed and photographed by inverted phase contrast microscopy. After cell cultures reached 70% confluency in 6-well plates, ADSCs (P4) were cultured in osteogenic medium for 21 days. Then cells were washed twice with PBS, fixed with paraformaldehyde for 20 min, stained with alizarin red staining solution for 30 min, washed with PBS, and observed and photographed by inverted phase contrast microscopy.

BMSCs (P4) were harvested by digestion with 0.25% trypsin with 0.02% EDTA, washed twice with PBS containing 0.1% sodium azide and 0.5% BSA, and resuspended in PBS at a density of 1×10^7 cells/ml. The cell suspension was incubated with AFR647-conjugated CD90 primary antibody or PE-conjugated CD45 primary antibody for 30 min at 4 °C in the dark. The antibody solution was then removed and the cells were resuspended in PBS without BSA and identified by flow cytometry.

Materials	Companies' supplier
Collagenase I	Gibco, Waltham, MA, USA
DMEM/F12	Hyclone, Logan, Utah, USA
FBS	Thermo Fisher Scientific, Rockford, IL, USA
CCK-8	Beyotime biotechnology, Shanghai, China
PBS	Hyclone, Logan, Utah, USA
0.25% trypsin	Gibco, Waltham, MA, USA
Adipogenic medium	Thermo Fisher Scientific, Rockford, IL, USA
Chondrogenic medium	Thermo Fisher Scientific, Rockford, IL, USA
Osteogenic medium	Thermo Fisher Scientific, Rockford, IL, USA
Oil red O staining solution	Solarbio life sciences, Beijing, China
Alize blue staining kit	Solarbio life sciences, Beijing, China
Alizarin red staining solution	Solarbio life sciences, Beijing, China
CD45 antibody	R&D Systems, Minneapolis, MN, USA
CD90 antibody	Novus Biologicals, Littleton, CO, USA
0.22-μm pore filters	Millipore, Temecula, CA, USA
Exosomal Protein Extraction Kit	FUJIFILM Wako Chemicals U.S.A. Corporation, Richmond, VA, USA
2.5% glutaraldehyde solution	Solarbio life sciences, Beijing, China
2% phosphotungstic acid solution	Solarbio life sciences, Beijing, China
CD9 primary antibody	Abcam, Waltham, MA, USA
CD63 primary antibody	PeproTech, Rocky Hill, NJ, USA
secondary antibodies for WB	Abcam, Waltham, MA, USA
PKH67	Sigma-Aldrich, St. Louis, MO, USA
BSA	Solarbio life sciences, Beijing, China
4% paraformaldehyde	Solarbio life sciences, Beijing, China
DAPI solution	Beyotime biotechnology, Shanghai, China
β-glycerophosphate	Sigma-Aldrich, St. Louis, MO, USA
dexamethasone	Sigma-Aldrich, St. Louis, MO, USA
ascorbic acid	Sigma-Aldrich, St. Louis, MO, USA
Triton X-100	National Drug Group Chemical Reagents Co., Ltd., Shanghai, China
Alkaline Phosphatase Assay Kit	Beyotime biotechnology, Shanghai, China
RIPA Lysis Buffer	Beyotime biotechnology, Shanghai, China
Skimmed milk	Beyotime biotechnology, Shanghai, China
PMSF	Beyotime biotechnology, Shanghai, China
RNAiso Plus	Takara Biomedical Technology, Beijing, China
PrimeScript™ RT reagent Kit	Takara Biomedical Technology, Beijing, China
Primers of GAPDH, COLA1, RUNX2 mRNA	Takara Biomedical Technology, Beijing, China
SYBR® Premix Ex Taq™ II	Takara Biomedical Technology, Beijing, China
nHA	Allgens Biotek, Inc., Beijing, China
Chitosan	Jinan Haidebei Marine Bioengineering Co., Ltd., Jinan, China
PLGA	Sigma-Aldrich, St. Louis, MO, USA
chloroform	National Drug Group Chemical Reagents Co., Ltd., Shanghai, China
sodium chloride	National Drug Group Chemical Reagents Co., Ltd., Shanghai, China
BCA protein assay kit	Beyotime biotechnology, Shanghai, China
anhydrous ethanol	National Drug Group Chemical Reagents Co., Ltd., Shanghai, China
1,1,1,3,3,3- hexamethyldisilazane	National Drug Group Chemical Reagents Co., Ltd.
penicillin	Provided by Department of local anatomy, The First Hospital of China Medical University
3% Sodium pentobarbital	Provided by Department of local anatomy, The First Hospital of China Medical University
Cyrazine hydrochloride	Provided by Department of local anatomy, The First Hospital of China Medical University
10% formalin	Solarbio life sciences, Beijing, China
EDTA decalcifying solution	Solarbio life sciences, Beijing, China
Paraffin wax	Solarbio life sciences, Beijing, China
Hematoxylin-Eosin (HE) Stain Kit	Solarbio life sciences, Beijing, China
Instruments	**Companies' supplier**
inverted phase contrast microscope	Olympus, Tokyo, Japan
thermostatic water bath	Beijing Tongde Venture Technology Co. , Ltd.
cell incubators	Thermo Fisher Scientific, Rockford, IL, USA
Continued	

Instruments	Companies' supplier
flow cytometry	BD Biosciences, San Jose, CA, USA
ultracentrifuge	Thermo Fisher Scientific, Rockford, IL, USA
transmission electron microscope	HITACHI, Ltd., Tokyo, Japan
confocal imaging system	Olympus, Tokyo, Japan
enzyme-labeled instrument	BioTek Instruments, Santa Clara, CA, USA
vertical electrophoresis apparatus	BIO-RAD, Hercules, CA, USA
ECL gel imaging system	Thermo Fisher Scientific, Rockford, IL, USA
spectrophotometer	Pierce, Rockford, IL, USA
Real-Time PCR Detection System	Applied Biosystems, Foster City, CA, USA
electronic balance	METTLER TOLEDO, Zurich, Switzerland
magnetic stirrer	Beijing Hongchangxin Technology Co. , Ltd.
scan electron microscope	HITACHI, Ltd., Tokyo, Japan
automated surgical fissure bur	STRONG, Daegu, Korea
vacuum desiccator	Merck KGaA, Darmstadt, Germany
X-ray scanning instrument	Siemens, Munich, Germany

Table 1. Materials and instruments used in methods.

Isolation of ADSC-derived exosomes

Log-phase ADSCs (passage 3) were supplemented with 10% exosome-free FBS, which was obtained by filtering the supernatants through 0.22-μm pore filters and ultracentrifuging at 100,000 g for 18 h. ADSCs cultured in the conditioned medium (DMEM containing 10% exosome-free FBS) were collected, and ADSC-derived exosomes (ADSC-EXOs) were harvested according to the protocol of the Exosomal Protein Extraction Kit. After fixation with glutaraldehyde, 10 μL of exosomes were dropped onto a copper mesh and then stained with 2% phosphotungstic acid solution for 2 min at room temperature. ADSC-EXO were observed by transmission electron microscopy. In addition, the exosomal markers CD63 and CD9 were identified by Western blotting. The protein of ADSCs or exosomes was extracted using RIPA Lysis Buffer plus 1mM phenylmethanesulfonyl fluoride (PMSF), and protein concentration was measured using the BCA protein assay kit. Equal amounts of protein samples (20 μg) extracted from cells and exosomes were added to SDS-PAGE gel lanes. Electrophoresis was then performed in a vertical electrophoresis unit with voltage and time set at 60 V for 30 min in the concentrating gel and voltage and time set at 100 V for 50 min in the separating gel. Protein blots in the gels were then transferred to PVDF membranes in transfer printing buffer at 100 V for 1 h. PVDF membranes were sequentially incubated with 5% nonfat milk at room temperature for 3 h, then incubated with CD9 and CD63 primary antibodies at 4℃ overnight, then incubated with secondary antibody at room temperature for 2 h. PVDF membranes were immersed in ECL working fluid, and protein bands were observed using an ECL gel imaging system.

Exosome uptake assay

ADSC-EXO was labeled with PKH67 to determine its uptake by BMSCs. According to the manufacturer's protocol, ADSC-EXO diluted in 1 mL Diluent C and 4 μL PKH67 dye diluted in 1 mL Diluent C were incubated together. After 4 min, 2 mL 0.5% BSA was added to complete the staining. The labeled ADSC-EXO was washed in PBS at 100,000 g for 1 h. The ADSC-EXO pellet was then incubated with BMSCs for 48 h. After incubation, the cells were washed twice with PBS followed by fixation in 4% paraformaldehyde for 10 min. 6-diamidino-2-phenylindole (DAPI) solution was used to stain nuclei. Images were captured using a confocal imaging system.

Induction of osteogenic differentiation

Exosomes were isolated from the supernatants of ADSCs after incubation in osteogenic medium (DMEM/F12 supplemented with 10% FBS plus 10 mM β-glycerophosphate, 100 nM dexamethasone, and 0.2 mM ascorbic acid) for 2 days. BMSCs were seeded in cell culture plates and then treated with osteogenic medium plus over 25 μg/ml of ADSC-derived exosomes for the corresponding period. The optimal time-point and concentration for ADSC-EXO referred to previous research[32]. Subsequent in vitro and in vivo assays were performed as follows.

Cell proliferation assay

Cell proliferation of BMSCs in 96-well plates was evaluated using the Cell Counting Kit-8 (CCK-8) according to the manufacturer's instructions, and growth curves were plotted using absorbance values up to 7 days of incubation.

Mineralized nodules assay

The mineralized nodules of BMSCs in 24-well plates were stained with alizarin red staining solution after 21 days of incubation and then observed under a microscope.

Alkaline phosphatase (ALP) activity assay

After 21 days of incubation in 6-well plates, BMSCs protein was extracted by being immersed in 0.05% Triton X-100 at 4 ° C overnight, then sonicated (150 W, 250 s) in an ice bath and centrifugated (4 ° C, 12000 g, 15 min).

According to the manufacturer's protocol of Alkaline Phosphatase Assay Kit, 50 μl protein samples and 50 μl para-nitrophenyl phosphate (pNPP) were added to 96-well plates, followed by incubation at 37℃ for 30 min. After the addition of 100 μl of termination reaction solution, the optical density was detected using a microplate reader at a wavelength of 405 nm. ALP activity was expressed in DEA activity units, which can be calculated according to the formula derived from the concentration and optical density of standards per unit time.

Quantitative real-time PCR (qRT-PCR) assay

After 21 days of incubation in 6-well plates, BMSCs total RNA was extracted using RNAiso Plus, then the concentration of RNA was measured using a spectrophotometer. The reverse transcriptase reaction was performed using PrimeScript™ RT reagent Kit, and the resulting cDNA was used for subsequent real-time PCR using a 7500 Real-Time PCR Detection System with SYBR® Premix Ex Taq™ II kit. GAPDH was used as an internal control, the sequences of the primers for GAPDH, collagen type I alpha 1 (COL1A1) and runt-related transcription factor 2 (RUNX2) used in this study are shown in Table 2.

Preparation of ADSC-EXO-loaded nHA/CS/PLGA scaffolds

The scaffolds were prepared by the particle leaching method at room temperature. nHA (particle size: 20–40 nm), Chitosan (CS, deacetylation 93%), and PLGA (MW 66,000-107,000 Da, PGA/PLA ratio = 25:75) were prepared in the weight ratio of 10:10:80. PLGA was completely dissolved in chloroform and adjusted to 10% concentration. Then, nHA and CS were added and stirred thoroughly. Sodium chloride (particle size between 150 and 250 μm) was added to the suspension in the volume ratio of 1:10. The mixture was uniformly stirred, ultrasonically degassed, and then poured into a Teflon mold. After static placement for 24–48 h, the scaffolds were demolded and statically placed again for 24–48 h. The scaffolds were then dried in a vacuum box for 24 h, then immersed in deionized water and stirred at intervals for 48 h, with deionized water replaced every 4–6 h. Finally, the scaffolds were sequentially dried in atmosphere and vacuum for 48 h, then they were broken into small segments and observed by scanning electron microscope (SEM) after being sputter-coated with gold.

The scaffolds were sterilized with oxirane prior to application. To immobilize with exosomes, nHA/CS/PLGA scaffolds were immersed in 1 μg/μl exosomes solution (250 μl/scaffold) for 12 h at 4 °C. To measure exosome release, nHA/CS/PLGA-EXO scaffolds were immersed in PBS and then placed in a cell incubator for 9 days. Supernatants were collected to measure the quantity of exosomes released using a BCA protein assay kit. To measure biocompatibility of nHA/CS/PLGA scaffolds, BMSCs were inoculated into the scaffolds then placed in a cell incubator for 5 days. Cell-scaffold complexes were gently washed with PBS, then fixed with 2.5% glutaraldehyde at 4 °C overnight. The samples were then dehydrated gradually through gradient concentrations of ethanol (30%, 50%, 70%, 80%, 90%, 100%, 100%, 5 min for each immersion) and finally treated with 1,1,1,3,3,3-hexamethyldisilazane (C6H19NSi2) for 10 min. After air drying, the samples were sputter-coated with gold and examined by SEM.

In vivo experiments

The rabbit mandibular bone defect model was established. Briefly, healthy 4–6 month old New Zealand rabbits ($n = 24$) were randomized into the control group ($n = 6$, no scaffolds), graft group ($n = 6$, filled with nHA/CS/PLGA scaffolds only), graft-EXO group ($n = 6$, filled with exosome-loaded nHA/CS/PLGA scaffolds), graft-EXO group ($n = 6$, filled with exosome-loaded nHA/CS/PLGA scaffolds), and graft-EXO + BMSCs group ($n = 6$, filled with exosome-loaded nHA/CS/PLGA scaffolds and BMSCs). Rabbits were anesthetized and then incised in parallel over the bilateral submandibular area. Muscle and periosteum were bluntly dissected, then a full-thickness bony defect of 8 mm diameter was created in the middle segment of the mandible on each side using an automated surgical fissure drill. The nHA/CS/PLGA-EXO scaffolds or nHA/CS/PLGA scaffolds were applied to the defect region, BMSCs were suspended in PBS (1×10^8/ml) and slowly applied to the defect region using a syringe (Fig. 2), followed by suturing the incision layer by layer. Rabbits were observed for complications or abnormal behavior and treated with penicillin at a dose of 80,000 IU once daily for 3 days. At postoperative weeks 4, 8, and 12, two rabbits in each group were sacrificed by aeroembolism and then examined.

X-Ray examination and histologic examination

To monitor the healing status of the bony defect, the mandibles were removed from rabbits and scanned with an X-ray scanning instrument. After being fixed in 10% formalin, the specimens were decalcified in 10% EDTA (pH 7.0) at 4℃ for 3 weeks. Then the specimens were embedded in paraffin and cut into 5 μm serial tissue sections. The tissue sections were deparaffinized and stained with hematoxylin-eosin (HE) staining kit, then observed using a microscope.

COL1A1	forward: 5'- TAAAGGGTCACCGTGGCTTC – 3'
	reverse: 5'- GAGGCCGTTGAGTCCATCTT – 3'
RUNX2	forward: 5'-TATGAAAAACCAAGTAGCAAGGTTC-3'
	reverse: 5'-GTAATCTGACTCTGTCCTTGTGGAT-3'
GAPDH	forward: 5'- TGGAATCCACTGGCGTCTTC-3'
	reverse: 5'- GGTTCACGCCCATCACAAAC – 3'

Table 2. Sequences of primers used in this study.

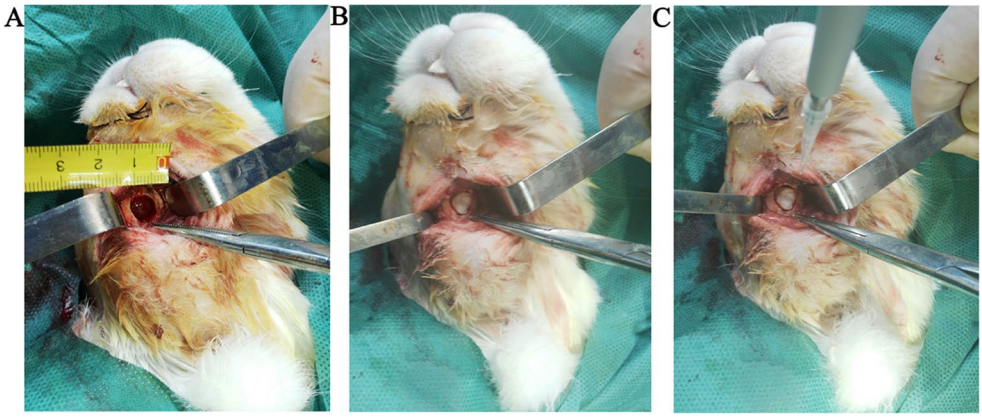

Figure 2. Operation procedure. Preparation of critical mandibular bone defect of rabbits (**A**), filling nHA// CS/PLGA-EXO scaffolds into defect cavity (**B**), dripping BMSCs into defect cavity (**C**).

Statistical analysis

All data are presented as mean ± standard deviation (SD). SPSS 29.0 and GraphPad Prism 5.0 were used for data analysis. Statistical analyses between two groups were performed using Student's t-test. Differences were considered statistically significant at $P < 0.05$.

Results

Characterization and of ADSC and BMSCs

The morphology of isolated ADSCs was long and spindle-shaped with the nucleus in the middle, and the cell border was clear (Fig. 3A). The morphology of isolated BMSCs was small and spindle-shaped with a large nucleus (Fig. 3B). After 28 days of chondrogenic induction, ADSCs tightly aggregated into a visible mass with enormous mucin sulfate in the cytoplasm and extracellular matrix, which can be stained light blue with Alcian dye (Fig. 3C). After 14 days of adipogenic induction, ADSCs were enlarged and filled with multiple visible lipid droplets that could be stained bright red with oil red o dye (Fig. 3D). After 21 days of osteogenic induction, ADSCs were enlarged and arranged in a turbo-like shape with multiple visible calcium nodules in the extracellular matrix, which can be stained orange-red with Alizarin red dye (Fig. 3E). Flow cytometry results of undifferentiated BMSCs (P4) confirmed positive expression of stromal stem cell marker CD90 (94.2%) and negative expression of endothelial progenitor cell marker CD45 (0.6%) (Fig. 3F).

ADSC-EXO identification and internalization by BMSCs

The isolated ADSC-EXO were typical small double concave disk-shaped nanoparticles with a diameter of 30 to 150 nm by transmission electron microscopy (Fig. 4A). Western blotting confirmed the expression of exosome-specific biomarkers CD9 and CD63 (Fig. 4B). After 48 h co-culture, fluorescence staining showed that PKH67-labeled ADSC-EXO were internalized and distributed in the perinuclear region of BMSCs (Fig. 4C).

Efficacy of ADSC-EXO on BMSCs

Cell proliferation of BMSCs treated with ADSC-EXO was much higher than that of BMSCs treated without ADSC-EXO from 3rd day to 7th day ($P < 0.01$, Fig. 5A; Table 3), osteogenesis of BMSCs treated with ADSC-EXO was also promoted as the formation of mineralized nodules increased (Fig. 5B&C). Meanwhile, osteogenic biomarkers of BMSCs, including ALP activity (Fig. 5D; Table 4), and COL1A1 (Fig. 5E; Table 4), RUNX2 (Fig. 5F; Table 4) mRNA levels were significantly increased after co-culture with ADSC-EXO ($P < 0.01$).

Characterization of nHA/CS/PLGA scaffolds

The nHA/CS/PLGA scaffolds exhibited a cylindrical shape with a diameter of 0.8 cm and a height of 0.4 cm and a foamy surface (Fig. 6A). Under SEM observation, the nHA/CS/PLGA scaffolds showed a three-dimensional porous structure with pore sizes ranging from 10 μm to 300 μm (Fig. 6B), and the pore wall showed a rough appearance with scattered nHA or CS grains (Fig. 6C). The total quantity of immobilized exosomes was 136.04 ± 8.73 μg on each nHA/CS/PLGA scaffold. The immobilized exosomes showed a burst release during the first 3 days and a slow release during the following 6 days (Fig. 6D; Table 5). After inoculation into the scaffolds for 5 days, numerous spindle-shaped BMSCs overlapped each other and covered the surface of the pore wall under SEM (Fig. 6. E).

nHA/CS/PLGA-EXO scaffolds repair maxillofacial osseous defects in vivo

At postoperative 4th week, the bone defect cavities were not narrowed in the control and graft groups, whereas slight narrowing with blurred contours was observed in the graft-EXO and graft-EXO + BMSCs groups under radiographic observation (Fig. 7a1-d1). Under microscopic observation of HE-stained sections, the contours of the bone defect cavities were clearly visible, and the cavities were filled with fibrin in the control group; the edges of the bone defect cavities were loosely attached to the scaffolds, and numerous fibrin and erythrocytes

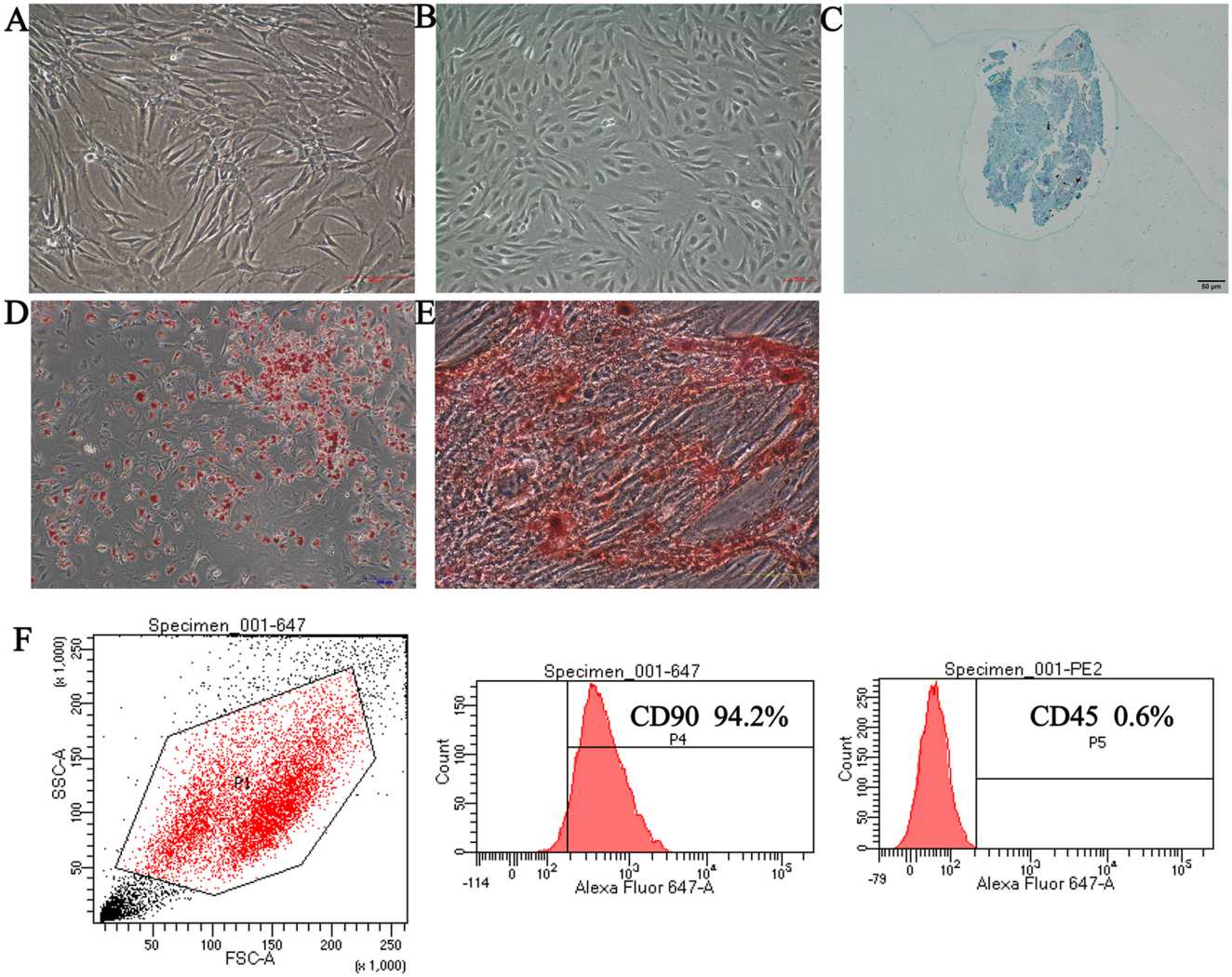

Figure 3. Characterization and identification of ADSCs and BMSCs. Cellular morphology of isolated ADSCs (**A**) and BMSCs (**B**). Alize blue staining (**C**), Oil red O staining (**D**), and Alizarin red staining (**E**) of isolated ADSCs undergoing chondrogenesis, adipogenesis, and osteogenesis respectively. Positive expression of stromal stem cell markers CD90 (94.2%), and negative expression of endothelial progenitor cell marker CD45 (0.6%) in undifferentiated BMSCs (**F**).

were observed in the scaffold pores in the graft group; The scaffolds infiltrated into the surrounding tissues in the graft-EXO group and graft-EXO + BMSCs group, and small areas of newborn bone and blood vessels were scattered in the "fusion area" in the graft-EXO + BMSCs group. (Figure. 8a1-d1).

At postoperative 8th week, the bone defect cavities had not narrowed in the control group, whereas slight narrowing was observed in the graft group and significant narrowing in the graft-EXO and graft-EXO + BMSCs groups under radiographic observation (Fig. 7a2-d2). Under microscopic observation of HE-stained sections, the contours of the bone defect cavities remained clear in the control group, the scaffolds were deformed and loosely connected with the surrounding tissues in the graft group, the scaffolds collapsed and embedded in the surrounding tissues, newborn osteoid was scattered in the cavities, and a large number of osteoblasts and blood vessels were observed in the graft-EXO group and graft-EXO + BMSCs group. (Figure. 8a2-d2).

At the 12th postoperative week, bone defect cavities still existed in the control group, while the entire cavities were blurred in the graft group, and the cavities almost disappeared in the graft-EXO group and graft-EXO + BMSCs group under radiographic observation (Fig. 7a3-d3). Under microscopic observation of HE-stained sections, the contours of the bone defect cavities remained clear, and the mass of fibrin and erythrocytes shrank significantly in the control group; the scaffolds almost disappeared and were replaced by a large amount of fibrous connective tissue and a few blood vessels in the graft group; The scaffolds completely degraded and were replaced by a large amount of neonatal bone and blood vessels in the graft-EXO and graft-EXO + BMSCs groups, while osteoid predominated in the graft-EXO group and lamellar bone predominated in the graft-EXO + BMSCs group (Fig. 8a3-d3).

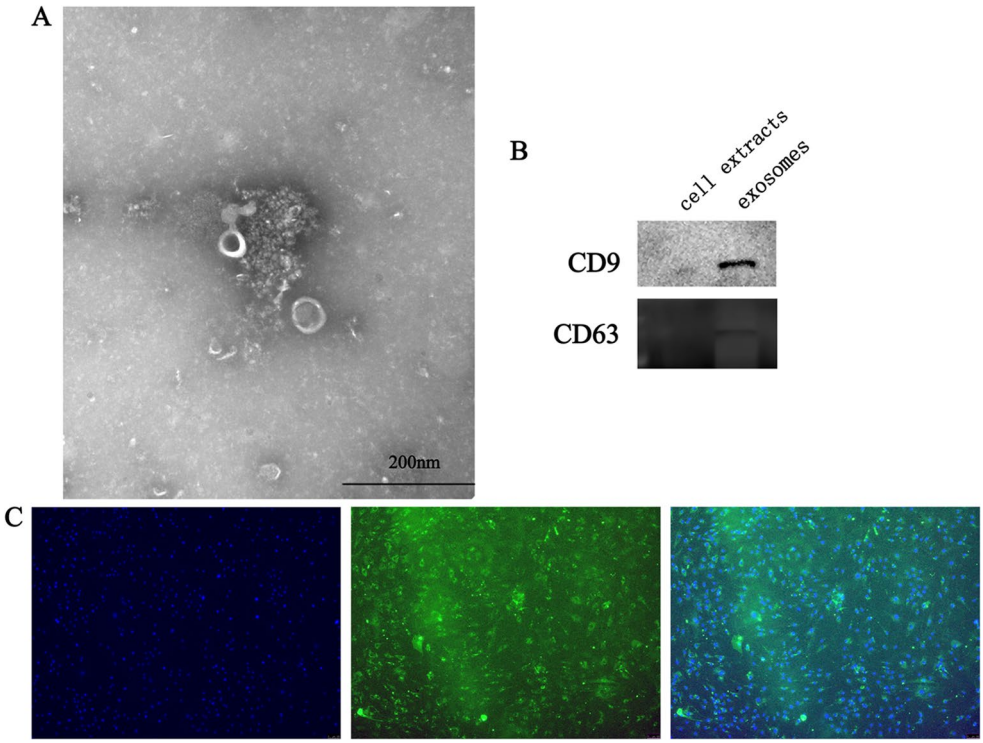

Figure 4. ADSC-EXO identification and internalization by BMSCs. The morphology of isolated ADSC-derived exosomes (ADSC-EXO) under transmission electron microscope (**A**). Protein expression of exosome-specific biomarkers CD9 and CD63 in exosomes and ADSCs samples (**B**). Immunofluorescent staining traced internalization of PKH67 labeled ADSC-EXO by BMSCs (**C**), the left photo displayed DAPI- stained nuclei, the middle photo displayed PKH67 labeled ADSC-EXO in the perinuclear region of BMSCs, the right photo was the merge of the left and middle photo.

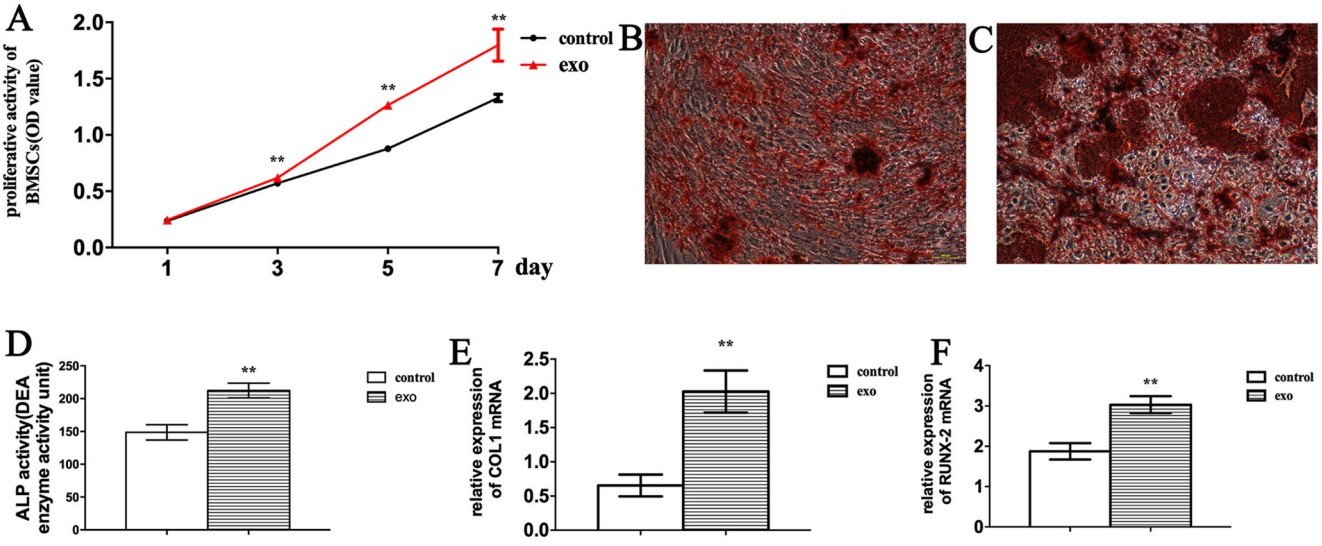

Figure 5. Efficacy of ADSC-EXO on BMSCs. (**A**) Cell proliferation of BMSCs treated with ADSC-EXO was much higher than that of BMSCs treated without ADSC-EXO from 3rd day. Alizarin red staining of BMSCs treated with osteogenic medium (**B**) and BMSCs treated with osteogenic medium plus ADSC-EXO (**C**). The osteogenic biomarkers, including ALP activity (**D**), COL1A (**E**), and RUNX2 (**F**) mRNA levels expression of BMSCs treated with osteogenic medium plus ADSC-EXO were much higher than that of BMSCs treated only with osteogenic medium.

Time(days)	Control group	ADSC-EXO group
1	0.2361 ± 0.0184	0.2434 ± 0.0752
3	0.5700 ± 0.0198	0.6199 ± 0.0165**
5	0.8775 ± 0.0131	1.2638 ± 0.0088**
7	1.3290 ± 0.0321	1.7968 ± 0.1430**

Table 3. Proliferative activity (absorbance) of BMSCs. Values are mean ± sd. $^{**}P < 0.01$ compared with control group.

	Control group	ADSC-EXO group
ALP activity	148.5699 ± 11.6739	212.4219 ± 11.3156**
COL1A1 mRNA	0.6542 ± 0.1584	2.0278 ± 0.3071**
RUNX2 mRNA	1.8750 ± 0.6139	3.0328 ± 0.6355**

Table 4. ALP activity (DEA enzyme activity unit), relative expression of *COL1A1*and *RUNX2* mRNA level of osteogenic BMSCs. Values are mean ± sd. $^{**}P < 0.01$ compared with control group.

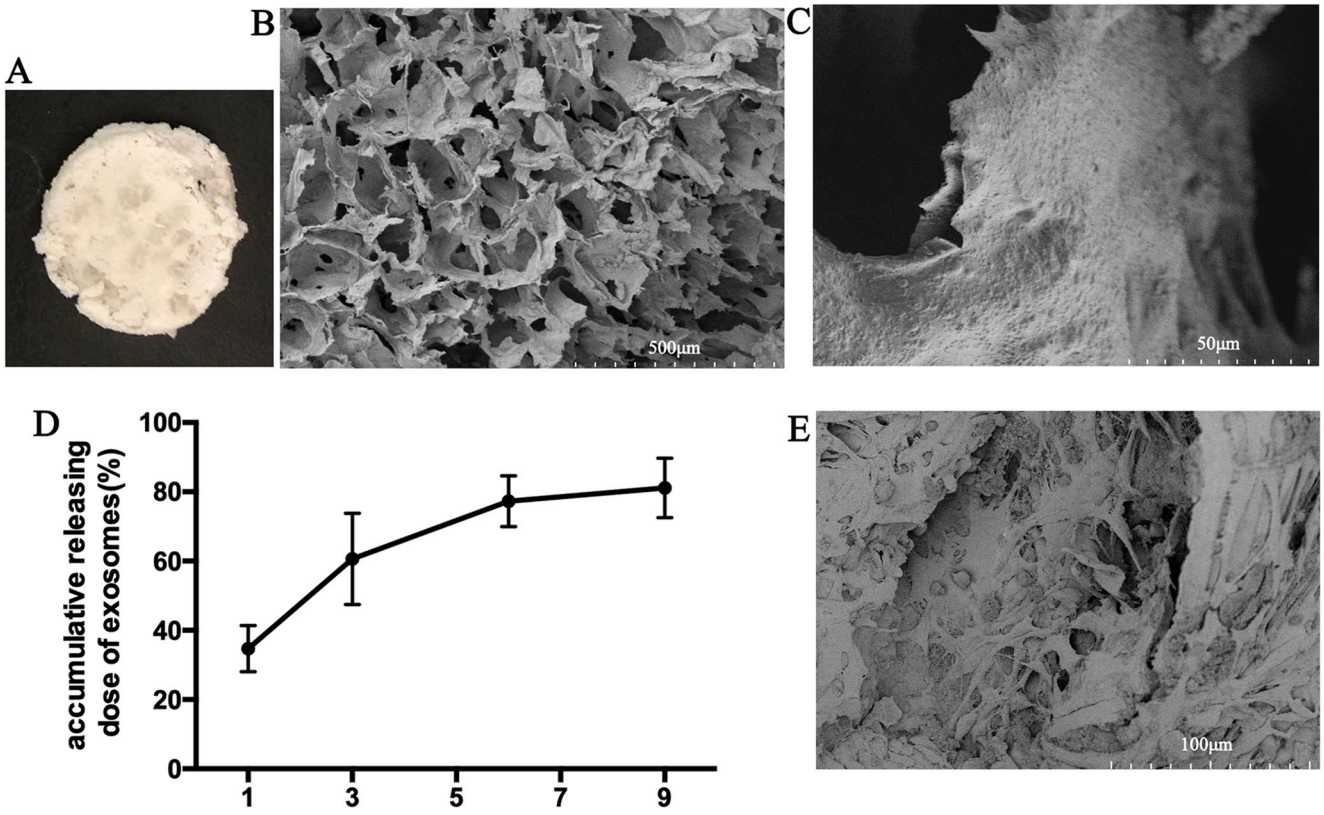

Figure 6. Characterization of nHA/CS/PLGA scaffolds. The general appearance (**A**) and surface topography under SEM (**B**, **C**) of nHA/CS/PLGA scaffolds. (**D**) In vitro exosomes release kinetics in PBS from nHA/CS/PLGA scaffolds. (**E**) Surface topography of BMSCs- loaded nHA/CS/PLGA scaffolds under SEM.

Discussion

Exosomes have the capacity to load multiple bioactive components involved in the regulation of cellular communication and function in a paracrine manner. Consequently, they have been combined with cells and materials to establish active tissue engineering complexes, which represent a promising future treatment for injured or defective tissues[33]. In the present study, we fabricated ADSC-EXO-loaded nHA/CS/PLGA scaffolds in combination with BMSCs for the repair of maxillofacial bone defects in rabbits. The results of this study suggest that this active tissue engineering bone may represent a promising therapeutic strategy for bone defects.

Exosomes represent a subset of extracellular vesicles derived from endosomes and subsequently released into the extracellular milieu following the fusion of multivesicular bodies with the plasma membrane. They are

Time(days)	Quantity of exosome
1	47.2370 ± 9.1023
3	82.5304 ± 17.9139
6	105.1639 ± 10.0030
9	110.3870 ± 11.7519

Table 5. Accumulative release of ADSC-derived exosomes (μg) from scaffold until 9th day($\bar{x} \pm s$, $n = 5$). Values are mean ± sd.

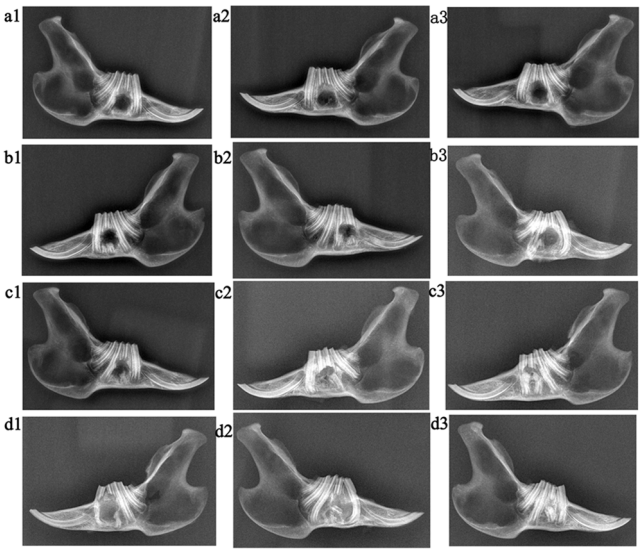

Figure 7. X-Ray observation of mandibular samples. X-Ray images of the bone defect cavities (a, control group; b, graft group; c, graft-EXO group; d, graft-EXO + BMSC group.1, 4 weeks after operation; 2, 8 weeks after operation; 3, 12 weeks after operation).

distributed in the majority of body fluids[34]. The function of exosomes is primarily contingent upon their contents, which includes nucleic acids, proteins, and lipids, in addition to the cell type of origin and the microenvironment[35]. As has been documented, ADSCs are capable of releasing exosomes that facilitate osteogenic differentiation[36,37]. These findings are consistent with those of previous studies, which have demonstrated that ADSC-EXOs significantly enhance the osteogenic differentiation of BMSCs. Tan et al. has demonstrated that local injection of ADSC-EXOs can recruit BMSCs and promote osteogenesis, chondrogenesis, and bone-tendon healing in both in vitro and in vivo models[38]. Li et al. found that exosomes secreted from human microvascular endothelial cells (HMEC-1) facilitated the osteogenic differentiation of BMSCs while simultaneously inhibiting the adipogenic differentiation process. This was achieved through the action of miR-5p-72106_14, which targeted and inhibited the STAT1 protein[39]. Chen et al. reported that M2-like macrophage-derived exosomes can upregulate the expression of IL-10 cytokines in BMSCs by directly delivering IL-10 mRNA, thereby activating the cellular IL-10/IL-10R pathway and promoting osteogenic differentiation of BMSCs[40]. Pu et al.. revealed that ubiquitin carboxyl-terminal hydrolase isozyme L3 (UCHL3) was enriched in mechanical force-induced macrophage-derived exosomes and exhibited a stronger ability to enhance BMSCs osteogenesis by targeting decapentaplegic homologue 1 (SMAD1)[41]. In light of these findings, we postulated that the isolated ADSC-EXOs may contain osteogenic proteins and RNAs that could facilitate osteogenesis in BMSCs independently of ADSCs.

In order for a given scaffold, whether natural or synthetic, to be successfully applied in the field of bone tissue engineering, it must meet a number of criteria. First, the degradation products of the scaffolds and their components must be non-toxic to the cells or biochemical factors that are loaded onto them. Second, the scaffolds must exhibit robust osteoinductive properties to facilitate the regeneration of bone tissue by the seeded cells or surrounding tissues. Third, the implanted scaffolds must evade recognition or attack by the immune system. The nHA/CS/PLGA scaffolds fabricated satisfy these fundamental requirements. In accordance with prior research[42,43], these scaffolds contain analogous components, structures, and biomechanical properties as those observed in natural bone matrix, and enhance the proliferation and osteogenic differentiation of BMSCs. Furthermore, nHA/CS/PLGA scaffolds have been demonstrated to facilitate the reconstitution of a physiological microenvironment for seeded cells, thereby preserving the stemness and functionality of mesenchymal stem cells through the activation of pertinent genes[44]. It can thus be ensured that the implanted BMSCs will be able to fully release their capabilities. It is well established that in the process of bone repair and regeneration, endogenous MSCs can be chemotactically recruited to the injury site and function as the primary healing cells[45,46]. It is

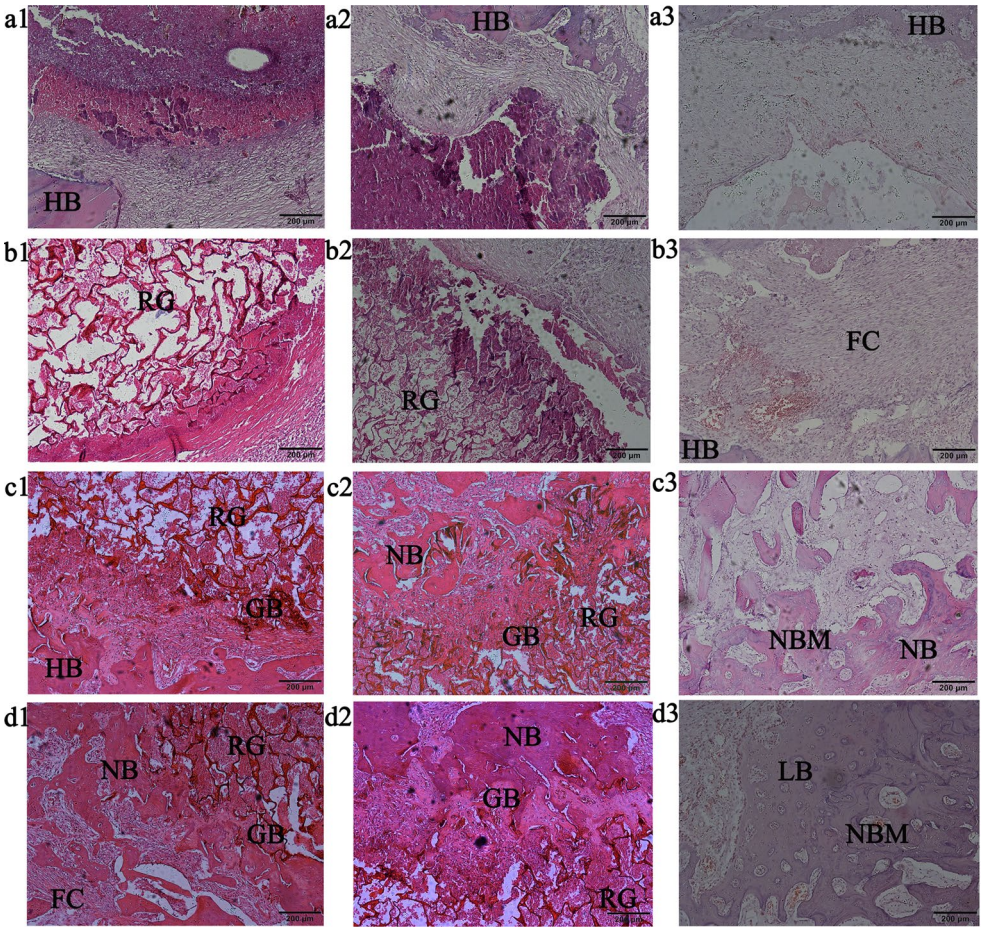

Figure 8. Histological observation of mandibular HE staining sections. HE staining of mandibular sections observation under microscope (a, control group; b, graft group; c, graft-EXO group; d, graft-EXO + BMSC group.1, 4 weeks after operation; 2, 8 weeks after operation; 3, 12 weeks after operation). HB, GB, FC, NB, NBM, RG refer to the host bone, graft bone, fibrous callus, new bone, new bone marrow, and remaining graft, respectively.

anticipated that the direct implantation of BMSCs into the defect will facilitate more expedient chemotactic homing, proliferation, and osteogenic differentiation in response to the released exosomes. Within the scaffold, nHA and CS were co-dispersed and coated the PLGA matrix. The hydrophilic environment, polar reaction, and hydrogen bonding among these molecules facilitate the absorption and maintenance of exosome stability[42,43]. As reported by Lan et al.., the exosomes enhanced chemotactic homing, adhesion and osteogenic differentiation, potentially through the activation of the RhoA/ROCK signaling pathway[47]. Our results indicated that the ADSC-EXO-loaded nHA/CS/PLGA scaffolds with BMSCs achieve satisfactory bone regeneration outcomes.

Prior research has employed the use of fibrin glue in conjunction with porous ceramic scaffolds and growth factors, which may exert a beneficial influence on the osteogenic and angiogenic processes in the repair of critical-size bone defects[48]. The utilization of lyophilized demineralized bovine bone granules in socket preservation to fill the extraction socket is of considerable importance for the maintenance of the dimensions of the alveolar bone. This is corroborated by the evidence of optimal soft and hard tissue healing observed in previous studies[49]. Furthermore, studies have investigated the impact of vascular endothelial growth factor (VEGF) supplementation on the expression of genes associated with osteogenesis and angiogenesis in dental stem cells. This approach represents a novel strategy for the promotion of bone and vascular regeneration in the context of tissue engineering[50]. Further investigation is required to elucidate the role of different types of scaffolds in osteogenic differentiation.

In conclusion, the findings of this study indicate that ADSC-EXOs can facilitate the osteogenic differentiation of BMSCs. Furthermore, the nHA/CS/PLGA scaffolds delivering ADSC-derived exosomes with BMSCs have the potential to facilitate the repair of critical-sized mandibular defects in rabbits. The findings of this study indicate that the treatment of maxillofacial bone defects may be effectively achieved through the use of the proposed approach.

Data availability

Data is provided within the manuscript or supplementary information files.

Received: 30 May 2024; Accepted: 16 October 2024
Published online: 11 November 2024

References

1. Ma, J. et al. Novel 3D printed TPMS scaffolds: microstructure, characteristics and applications in bone regeneration. *J. Tissue Eng.* **15**, 20417314241263689. https://doi.org/10.1177/20417314241263689 (2024).
2. Wei, J. et al. Significance and considerations of establishing standardized critical values for critical size defects in animal models of bone tissue regeneration. *Heliyon*. **10**, e33768. https://doi.org/10.1016/j.heliyon.2024.e33768 (2024).
3. Fabio, P., Mario, A. & Mirko Andreasi, B. Hard and soft tissue augmentation with occlusive titanium barriers in jaw vertical defects: a novel approach. *Plast. Aesthetic Res.* **9**, 7. https://doi.org/10.20517/2347-9264.2021.32 (2022).
4. Wang, J. et al. Application of Antioxidant Compounds in Bone Defect Repair. *Antioxid. (Basel)* 13. https://doi.org/10.3390/antiox13070789 (2024).
5. Jeffrey, S. M. & George, M. K. Point-of-care three-dimensional printing for craniomaxillofacial trauma. *Plast. Aesthetic Res.* **8**, 28. https://doi.org/10.20517/2347-9264.2020.222 (2021).
6. Li, N. et al. Advances in biomaterials for oral-maxillofacial bone regeneration: spotlight on periodontal and alveolar bone strategies. *Regen Biomater.* **11**, rbae078. https://doi.org/10.1093/rb/rbae078 (2024).
7. Galli, M., Yao, Y., Giannobile, W. V. & Wang, H. L. Current and future trends in periodontal tissue engineering and bone regeneration. *Plast. Aesthet. Res.* **8** https://doi.org/10.20517/2347-9264.2020.176 (2021).
8. Deng, J. et al. Versatile hypoxic extracellular vesicles Laden in an Injectable and Bioactive Hydrogel for Accelerated Bone Regeneration. *Adv. Funct. Mater.* **33**, 2211664. https://doi.org/10.1002/adfm.202211664 (2023).
9. Fan, J. Z. et al. Estrogen improves the proliferation and differentiation of hBMSCs derived from postmenopausal osteoporosis through notch signaling pathway. *Mol. Cell. Biochem.* **392**, 85–93. https://doi.org/10.1007/s11010-014-2021-7 (2014).
10. Lau, C. S. et al. Role of adipose-derived mesenchymal stem cells in bone regeneration. *Int. J. Mol. Sci.* **25** https://doi.org/10.3390/ijms25126805 (2024).
11. Tao, S. C. & Guo, S. C. Extracellular vesicles in bone: dogrobbers in the eternal battle field. *Cell. Commun. Signal.* **17**, 6–6. https://doi.org/10.1186/s12964-019-0319-5 (2019).
12. Prasad, P. & Cancelas, J. A. From marrow to bone and Fat: exploring the multifaceted roles of leptin receptor positive bone marrow mesenchymal stromal cells. *Cells*. **13** https://doi.org/10.3390/cells13110910 (2024).
13. Wu, Y. et al. Evaluation of Osteogenesis and Angiogenesis of Icariin in local controlled release and systemic delivery for calvarial defect in Ovariectomized rats. *Sci. Rep.* **7**, 5077–5077. https://doi.org/10.1038/s41598-017-05392-z (2017).
14. Shen, J. et al. Osteogenic mechanism of chlorogenic acid and its application in clinical practice. *Front. Pharmacol.* **15**, 1396354. https://doi.org/10.3389/fphar.2024.1396354 (2024).
15. Liu, Y. S. et al. The effect of simvastatin on chemotactic capability of SDF-1α and the promotion of bone regeneration. *Biomaterials*. **35**, 4489–4498. https://doi.org/10.1016/j.biomaterials.2014.02.025 (2014).
16. Zhao, W., Jin, K., Li, J., Qiu, X. & Li, S. Delivery of stromal cell-derived factor 1α for in situ tissue regeneration. *J. Biol. Eng.* **11**, 22–22. https://doi.org/10.1186/s13036-017-0058-3 (2017).
17. Liu, X., Dong, Y., Wang, C. & Guo, Z. Application of chitosan as nano carrier in the treatment of inflammatory bowel disease. *Int. J. Biol. Macromol.* 134899. https://doi.org/10.1016/j.ijbiomac.2024.134899 (2024).
18. Jamalpoor, Z. et al. Fabrication of cancellous biomimetic chitosan-based nanocomposite scaffolds applying a combinational method for bone tissue engineering. *J. Biomed. Mater. Res. A*. **103**, 1882–1892. https://doi.org/10.1002/jbm.a.35320 (2015).
19. Costa-Pinto, A. R., Reis, R. L. & Neves, N. M. Scaffolds based bone tissue engineering: the role of Chitosan. *Tissue Eng. Part. B Rev.* **17**, 331–347. https://doi.org/10.1089/ten.teb.2010.0704 (2011).
20. Zhou, H. & Lee, J. Nanoscale hydroxyapatite particles for bone tissue engineering. *Acta Biomater.* **7**, 2769–2781. https://doi.org/10.1016/j.actbio.2011.03.019 (2011).
21. Goto, T. et al. Resorption of synthetic porous hydroxyapatite and replacement by newly formed bone. *J. Orthop. Sci.* **6**, 444–447. https://doi.org/10.1007/s007760170013 (2001).
22. Seo, B. M. et al. Investigation of multipotent postnatal stem cells from human periodontal ligament. *Lancet*. **364**, 149–155. https://doi.org/10.1016/S0140-6736(04)16627-0 (2004).
23. Przekora, A. et al. Evaluation of the potential of chitosan/β-1,3-glucan/hydroxyapatite material as a scaffold for living bone graft production in vitro by comparison of ADSC and BMDSC behaviour on its surface. *Biomed. Mater.* **12**, 015030–015030. https://doi.org/10.1088/1748-605X/aa56f9 (2017).
24. Maria, A. T. J. et al. Adipose-derived mesenchymal stem cells in Autoimmune disorders: state of the art and perspectives for systemic sclerosis. *Clin. Rev. Allergy Immunol.* **52**, 234–259. https://doi.org/10.1007/s12016-016-8552-9 (2017).
25. He, C., Zheng, S., Luo, Y. & Wang, B. Exosome Theranostics: Biology and Translational Medicine. *Theranostics*. **8**, 237–255. https://doi.org/10.7150/thno.21945 (2018).
26. Boriachek, K. et al. Biological functions and current advances in isolation and detection strategies for Exosome Nanovesicles, Small (Weinheim an Der Bergstrasse. *Germany)*. **14** https://doi.org/10.1002/smll.201702153 (2018).
27. Narayanan, R., Huang, C. C. & Ravindran, S. Hijacking the Cellular Mail: Exosome mediated differentiation of mesenchymal stem cells. *Stem Cells Int.* **2016**, 3808674–3808674. https://doi.org/10.1155/2016/3808674 (2016).
28. Li, W. et al. Tissue-Engineered Bone immobilized with human adipose stem cells-derived Exosomes promotes bone regeneration. *ACS Appl. Mater. Interfaces*. **10**, 5240–5254. https://doi.org/10.1021/acsami.7b17620 (2018).
29. Ford, H. R., Jones, P., Gaines, B., Reblock, K. & Simpkins, D. L. Intraoperative handling and wound healing: controlled clinical trial comparing coated VICRYL plus antibacterial suture (coated polyglactin 910 suture with triclosan) with coated VICRYL suture (coated polyglactin 910 suture). *Surg. Infect. (Larchmt)*. **6**, 313–321. https://doi.org/10.1089/sur.2005.6.313 (2005).
30. Luo, L. et al. Fabrication of synthetic mesenchymal stem cells for the treatment of Acute myocardial infarction in mice. *Circul. Res.* **120**, 1768–1775. https://doi.org/10.1161/CIRCRESAHA.116.310374 (2017).
31. Zhao, D. et al. Poly(lactic-co-glycolic acid)-based composite bone-substitute materials. *Bioact Mater.* **6**, 346–360. https://doi.org/10.1016/j.bioactmat.2020.08.016 (2021).
32. Li, Q. et al. The tissue origin effect of extracellular vesicles on cartilage and bone regeneration. *Acta Biomater.* **125**, 253–266. https://doi.org/10.1016/j.actbio.2021.02.039 (2021).
33. Kim, H. D. et al. Biomimetic materials and fabrication approaches for bone tissue Engineering. *Adv. Healthc. Mater.* **6** https://doi.org/10.1002/adhm.201700612 (2017).
34. Yang, B., Chen, Y. & Shi, J. Exosome Biochemistry and Advanced Nanotechnology for Next-Generation Theranostic Platforms, Advanced materials (Deerfield Beach, Fla.). e1802896 (2018).
35. Whiteside, T. L. Exosome and mesenchymal stem cell cross-talk in the tumor microenvironment. *Semin. Immunol.* **35**, 69–79. https://doi.org/10.1016/j.smim.2017.12.003 (2018).
36. Yang, S., Guo, S., Tong, S. & Sun, X. Promoting osteogenic differentiation of human adipose-derived stem cells by altering the expression of Exosomal miRNA. *Stem Cells Int.* **2019**, 1351860–1351860. https://doi.org/10.1155/2019/1351860 (2019).
37. Zanicotti, D. G., Duncan, W. J., Seymour, G. J. & Coates, D. E. Effect of Titanium surfaces on the osteogenic differentiation of human adipose-derived stem cells. *Int. J. Oral Maxillofac. Implants*. **33**, e77–e87. https://doi.org/10.11607/jomi.5810 (2018).

38. Tan, X., Xiao, H., Yan, A., Li, M. & Wang, L. Effect of Exosomes from bone marrow-derived mesenchymal stromal cells and adipose-derived stromal cells on Bone-Tendon Healing in a murine Rotator Cuff Injury Model. *Orthop. J. Sports Med.* **12**, 23259671231210304. https://doi.org/10.1177/23259671231210304 (2024).
39. Li, H. et al. Exosome-derived miR-5p-72106_14 in vascular endothelial cells regulates fate determination of BMSCs. *Toxicol. Appl. Pharmacol.* **482**, 116793. https://doi.org/10.1016/j.taap.2023.116793 (2024).
40. Chen, X. et al. Exosomes derived from reparative M2-like macrophages prevent bone loss in murine periodontitis models via IL-10 mRNA. *J. Nanobiotechnol.* **20**, 110. https://doi.org/10.1186/s12951-022-01314-y (2022).
41. Pu, P. et al. Mechanical force induces macrophage-derived exosomal UCHL3 promoting bone marrow mesenchymal stem cell osteogenesis by targeting SMAD1. *J. Nanobiotechnol.* **21**, 88. https://doi.org/10.1186/s12951-023-01836-z (2023).
42. Wang, F., Zhang, Y. C., Zhou, H., Guo, Y. C. & Su, X. X. Evaluation of in vitro and in vivo osteogenic differentiation of nano-hydroxyapatite/chitosan/poly(lactide-co-glycolide) scaffolds with human umbilical cord mesenchymal stem cells. *J. Biomed. Mater. Res. A.* **102**, 760–768. https://doi.org/10.1002/jbm.a.34747 (2014).
43. Wang, F. et al. Bone regeneration by nanohydroxyapatite/chitosan/poly(lactide-co-glycolide) scaffolds seeded with human umbilical cord mesenchymal stem cells in the calvarial defects of the nude mice. *Biomed. Res. Int.* **2015**, 261938. https://doi.org/10.1155/2015/261938 (2015).
44. Su, X. et al. A bone matrix-simulating scaffold to alleviate replicative senescence of mesenchymal stem cells during long-term expansion. *J. Biomed. Mater. Res. A.* **108**, 1955–1967. https://doi.org/10.1002/jbm.a.36958 (2020).
45. Dimitriou, R., Tsiridis, E. & Giannoudis, P. V. Current concepts of molecular aspects of bone healing. *Injury.* **36**, 1392–1404. https://doi.org/10.1016/j.injury.2005.07.019 (2005).
46. Gerstenfeld, L. C., Cullinane, D. M., Barnes, G. L., Graves, D. T. & Einhorn, T. A. Fracture healing as a post-natal developmental process: molecular, spatial, and temporal aspects of its regulation. *J. Cell. Biochem.* **88**, 873–884. https://doi.org/10.1002/jcb.10435 (2003).
47. Díaz, E., Puerto, I., Ribeiro, S., Lanceros-Mendez, S. & Barandiarán, J. M. The Influence of Copolymer Composition on PLGA/nHA Scaffolds' Cytotoxicity and In Vitro Degradation. *Nanomaterials (Basel).* 7. https://doi.org/10.3390/nano7070173 (2017).
48. Enezei, H. H. et al. Osteoinductive activity of bone Scaffold Bioceramic Companied with Control Release of VEGF Protein Treated Dental stem cells as a New Concept for Bone Regeneration: part II. *J. Hard Tissue Biol.* **27**, 69–78. https://doi.org/10.2485/jhtb.27.69 (2018).
49. Al Qabbani, A. et al. Sheikh ab Hamid, three-Dimensional Radiological Assessment of alveolar bone volume preservation using bovine bone xenograft. *J. Craniofac. Surg.* **29**, e203–e209. https://doi.org/10.1097/scs.0000000000004263 (2018).
50. Enezei, H. H. et al. Enhanced osteogenic and angiogenic-related gene expression of Human Dental Stem cells on Biphasic Calcium Phosphate Scaffold Treated with vascular endothelial growth factor: part I. *J. Hard Tissue Biol.* **26**, 373–380. https://doi.org/10.2485/jhtb.26.373 (2017).

Acknowledgements

The present article enjoys supports from Key Laboratory for Immunology and Dermatology of Health's Ministry, the First Hospital of China Medical University.

Author contributions

Shu Guo designed the experiments. Ting Wang and Ye Zhang conducted the experiments. Ting Wang analyzed data.Ye Zhang prepared figures.Ting Wang and Shu Guo Wrote the main manuscript.All authors reviewed the manuscript.

Funding

This study was supported by the National Natural Science Foundation of China (Grant No.51872332) and Project of Liaoning Xingliao Talents Plan (XLYC2002103).

Declarations

Ethics approval and consent to participate

All animal experimental operations were approved by the China Medical University Committee for Laboratory Animal Welfare and Ethics (No. 2017036). All animal experiments were complied with the ARRIVE guidelines, and were carried out in accordance with the U.S. Public Health Service Policy on Humane Care and Use of Laboratory Animals.

Competing interests

The authors declare no competing interests.

Additional information

Supplementary Information The online version contains supplementary material available at https://doi.org/10.1038/s41598-024-76672-8.

Correspondence and requests for materials should be addressed to S.G.